The Astrophysical Journal, 951:85 (10pp), 2023 July 10 https://doi.org/10.3847/1538-4357/acd8ba

Modeling the Chemical Enrichment History of the Bulge Fossil Fragment Terzan 5

Donatella Romano[1], Francesco R. Ferraro[1,2], Livia Origlia[1], Simon Portegies Zwart[3], Barbara Lanzoni[1,2], Chiara Crociati[1,2], Davide Massari[1], Emanuele Dalessandro[1], Alessio Mucciarelli[1,2], R. Michael Rich[4], Francesco Calura[1], and Francesca Matteucci[5,6,7]
[1] INAF, Osservatorio di Astrofisica e Scienza dello Spazio, Via Gobetti 93/3, I-40129 Bologna, Italy; donatella.romano@inaf.it
[2] Dipartimento di Fisica e Astronomia, Università di Bologna, Via Gobetti 93/2, I-40129 Bologna, Italy
[3] Leiden Observatory, Leiden University, P.O. Box 9513, 2300 RA Leiden, The Netherlands
[4] Department of Physics and Astronomy, University of California, 90095 Los Angeles, CA, USA
[5] Sezione di Astronomia, Dipartimento di Fisica, Università di Trieste, Via Tiepolo 11, I-34143 Trieste, Italy
[6] INAF, Osservatorio Astronomico di Trieste, Via Tiepolo 11, I-34143 Trieste, Italy
[7] INFN, Sezione di Trieste, Via Valerio 2, I-34127 Trieste, Italy
Received 2023 March 15; revised 2023 May 5; accepted 2023 May 23; published 2023 July 5

Abstract

Terzan 5 is a heavily obscured stellar system located in the inner Galaxy. It has been postulated to be a stellar relic, a bulge fossil fragment witnessing the complex history of the assembly of the Milky Way bulge. In this paper, we follow the chemical enrichment of a set of putative progenitors of Terzan 5 to assess whether the chemical properties of this cluster fit within a formation scenario in which it is the remnant of a primordial building block of the bulge. We can explain the metallicity distribution function and the runs of different element-to-iron abundance ratios as functions of [Fe/H] derived from optical-infrared spectroscopy of giant stars in Terzan 5 by assuming that the cluster experienced two major star formation bursts separated by a long quiescent phase. We further predict that the most metal-rich stars in Terzan 5 are moderately He-enhanced, and we predict a large spread of He abundances in the cluster, $Y \simeq 0.26$–0.335. We conclude that current observations fit within a formation scenario in which Terzan 5 originated from a pristine or slightly metal-enriched gas clump about one order of magnitude more massive than its present-day mass. Losses of gas and stars played a major role in shaping Terzan 5 the way we see it now. The iron content of the youngest stellar population is better explained if the white dwarfs that give rise to type Ia supernovae (the main Fe factories) sink toward the cluster center, rather than being stripped by the strong tidal forces exerted by the Milky Way in the outer regions.

Unified Astronomy Thesaurus concepts: Galactic bulge (2041); Galactic archaeology (2178); Galaxy chemical evolution (580); Star clusters (1567); Stellar abundances (1577)

1. Introduction

The formation and evolution of bulges (encompassing classical bulges and pseudobulges; Kormendy & Kennicutt 2004) in massive spiral galaxies can be driven by several mechanisms, including violent early dissipative collapse of gas (Eggen et al. 1962), mergers (Springel & Hernquist 2005), secular evolution of dynamically unstable disks (Combes et al. 1990), coalescence of giant star-forming clumps (Immeli et al. 2004; Elmegreen et al. 2008), or a combination thereof (see Athanassoula 2005, for a review).

In our Galaxy, the bulge formation process is likely a motley growth, leading to a composite system. Although the central regions of the Milky Way (MW) are notoriously challenging to observe due to crowding and variable extinction on small spatial scales that severely hamper an unbiased view (Baade 1946; Gonzalez et al. 2012; Nogueras-Lara et al. 2021), it can be plainly argued that the Galactic bulge is a complex environment in which different stellar populations coexist (Bensby et al. 2013; Rojas-Arriagada et al. 2014; Barbuy et al. 2018; Horta et al. 2021; Queiroz et al. 2021; Nieuwmunster et al. 2023, see also Athanassoula et al. 2017).

In the past decades, deep photometry and high-resolution spectroscopy of large samples of individual stars have provided key information on the ages, kinematics, and chemical composition of the stellar populations inhabiting the MW bulge. The old ages inferred from color–magnitude diagrams (CMDs) of different globular clusters (GCs) and fields in the bulge (Ortolani et al. 1995; Zoccali et al. 2003; Clarkson et al. 2008; Valenti et al. 2013; Bica et al. 2016; Saracino et al. 2019; Surot et al. 2019) rule out an extended period of star formation. Yet, some stars with ages $\leqslant 5$ Gyr are present (e.g., Bensby et al. 2013, 2017; Catchpole et al. 2016; Schultheis et al. 2017). The significance of this young population is the subject of ongoing debate (Haywood et al. 2016; Renzini et al. 2018; Saha et al. 2019; Rich et al. 2020). Hasselquist et al. (2020) note that the likelihood of ending up with some relatively young stars in a bulge sample depends on the metallicity and height above the plane probed by the observations. Indeed, younger stars are found among the metal-richest stars and closer to the Galactic plane.

Field stars in the bulge cover a broad metallicity range, $-1.9 \leqslant$ [Fe/H] $\leqslant +0.6$ (Bensby et al. 2013), with a few extremely metal-poor stars at [Fe/H] < -3 (Howes et al. 2015). Metal-poor and metal-rich stars present distinct kinematic properties that are overall consistent with belonging to an old spheroid (or thick disk) and a buckled bar, respectively (Hill et al. 2011; Babusiaux 2016). In a [α/Fe]–[Fe/H] diagram, members of the old metal-poor pressure-supported spheroidal component dominate a well-defined upper sequence,

while objects inhabiting the metal-rich boxy/peanut X-shaped bar populate the lower sequence, which sets important constraints on the formation timescale of each component (Rojas-Arriagada et al. 2019). The complexity of the stellar populations further shows up in the metallicity distribution function (MDF), which unveils a clear multimodality[8] with varying proportions of its main components in different fields of view (Bensby et al. 2013; Rojas-Arriagada et al. 2020).

In terms of chemical properties, GCs in the bulge behave as their halo and thick-disk counterparts. Their members show the characteristic anticorrelations among the abundances of light elements, while the abundances of heavy elements do not present internal variations and follow the average abundance patterns traced by field stars (Gratton et al. 2019).

Clusters found in the inner Galaxy possibly had higher masses in the past. Likely, they have lost preferentially low-mass stars owing to mass segregation and strong tidal forces (Vesperini & Heggie 1997; Baumgardt & Makino 2003). These processes may eventually lead to the complete dissolution of the clusters (Portegies Zwart et al. 2002). Recently, Minniti et al. (2018) have reported the first clear observational signature of bulge-crossing shocks for M 62, one of the most massive MW GCs located in the bulge. Another important point is that in *N*-body calculations, the stellar remnants strongly concentrate toward the cluster core (e.g., Baumgardt & Makino 2003).

A few stellar systems in the MW bulge deserve special attention. In fact, up to now, two stellar systems in the MW bulge with the appearance of massive GCs, namely, Terzan 5 and Liller 1, have been found to harbor multiple subpopulations with large differences in age and in iron content (Ferraro et al. 2009, 2016, 2021). The modeling of the star formation history of Liller 1 suggests that this stellar system has been forming stars over its entire lifetime, with three main star formation episodes—the oldest occurring some 12–13 Gyr ago and the most recent episode occurring only 1–3 Gyr ago—and some low-level activity in between (Dalessandro et al. 2022). Indeed, the first spectroscopic screening of Liller 1 confirms the presence of multi-iron subpopulations (Crociati et al. 2023).

The case of Terzan 5, which is the target of this study, is observationally better constrained. Terzan 5 is a dense conglomeration of stars formerly classified as a GC, which is now known to harbor two main populations of stars, one old (age $=12\pm1$ Gyr) and relatively metal poor, with $[\mathrm{Fe/H}]_{\mathrm{peak}}=-0.25\pm0.07$ and $[\alpha/\mathrm{Fe}]=+0.34\pm0.06$, the other younger (age $=4.5\pm0.5$ Gyr) and metal rich, with $[\mathrm{Fe/H}]_{\mathrm{peak}}=+0.27\pm0.04$ and $[\alpha/\mathrm{Fe}]=+0.03\pm0.04$ (Ferraro et al. 2009, 2016; Origlia et al. 2011, 2013, 2019). A third minor component is also detected, peaking at $[\mathrm{Fe/H}]_{\mathrm{peak}}=-0.79\pm0.04$ and with $[\alpha/\mathrm{Fe}]=+0.36\pm0.04$ (Origlia et al. 2013; Massari et al. 2014). Although an additional ultra metal-rich component at $[\mathrm{Fe/H}]=+0.5$ could be possibly present, the statistics is still too low to firmly confirm its existence. The CMD analysis (Ferraro et al. 2009, 2016) and the reconstructed star formation history (C. Crociati et al. 2023, in preparation) clearly point to two major star formation events, separated by a long quiescent—or low-level activity—period. These characteristics definitely indicate that Terzan 5 had a more massive progenitor that was able to retain its supernova (SN) ejecta and self-enrich. Such an object would be seen as a giant star-forming clump at high redshift (Bournaud et al. 2008; Elmegreen et al. 2008). Interestingly, the peaks in the MDF of Terzan 5 closely track those in the MDF of the general bulge population, [Fe/H] $=+0.32$, -0.17, and -0.66 (Rojas-Arriagada et al. 2020). This would suggest a synchronous formation (Pflamm-Altenburg & Kroupa 2009; McKenzie & Bekki 2018), rather than the accretion of a satellite previously evolved in isolation (a scenario that instead explains the dynamical and chemical properties of another anomalous GC-like system rather well, ω Centauri; Bekki & Freeman 2003; Romano et al. 2007). Indeed, the orbit of Terzan 5 suggests an in situ origin (Massari et al. 2015; Baumgardt et al. 2019). Is it hence possible that a non-negligible fraction of bulge stars formed within gaseous cocoons that self-enriched and then disrupted, leaving behind a few compact survivors? Could Terzan 5 and Liller 1 be the remnants of these building blocks? In order to answer these questions, here we explore possible evolutionary paths yielding a stellar system whose structure and chemical properties are compatible with the present-day configuration of Terzan 5.

The layout of the paper is as follows. The chemical evolution model is described in Section 2. The results are compared to the available observations in Section 3. Predictions still awaiting the test of future observations are presented in Section 4 and are discussed in light of existing scenarios for the origin of Terzan 5. Our conclusions are drawn in Section 4.

2. Chemical Evolution Model

We follow the evolution of the abundances of several chemical elements representative of different nucleosynthesis channels (light, α, Fe-peak, and neutron-capture elements) in the interstellar medium (ISM) of putative precursors of Terzan 5. To this end, we use a single-zone numerical model (Romano & Starkenburg 2013; Romano et al. 2015) that solves the classical set of equations of chemical evolution (Tinsley 1980; Matteucci 2012, 2021).

We do not implement any detailed treatment of the gas and star dynamics in our model. Nonetheless, we are able to discuss some dynamical effects by placing our findings into the broader context provided by *N*-body simulations of star cluster evolution (see Sections 3 and 4).

2.1. Basic Assumptions

Raw material for star formation is provided by gas cooling within a giant cloud (for a thorough discussion of gas accretion modes in galaxies, see Sánchez Almeida et al. 2014). We consider either pristine gas with a primordial chemical composition ($Z_{\mathrm{in}}=0$) or pre-enriched gas with $[\mathrm{Fe/H}]=-1$ ($Z_{\mathrm{in}}\simeq0.005$). The rate of gas infall is parameterized as

$$\frac{dM_{\mathrm{in}}}{dt}\propto \mathrm{e}^{-t/\tau}, \tag{1}$$

where M_{in} is the initial mass of the cloud, and the e-folding time, τ, is a free parameter of the model.

The cold gas is turned into stars following a phenomenological law (Schmidt 1959; Kennicutt 1998),

$$\psi(t)=\nu M_{\mathrm{gas}}^{k}(t), \tag{2}$$

where the star formation efficiency, ν, is a free parameter of the model (set constant in time) and $k=1$.

[8] Other works (Bensby et al. 2011; Hill et al. 2011; Rojas-Arriagada et al. 2014; Gonzalez et al. 2015; Zoccali et al. 2017; Schultheis et al. 2017) reveal a bimodality in the MDF that is possibly due to smaller sample sizes and/or larger individual measurement errors.

The multipeaked MDF and CMD morphology of Terzan 5 suggest that the star formation in the protocluster was not a smooth, continuous process, but rather proceeded through distinct bursts (Ferraro et al. 2016), possibly interspersed with low-level activity, as is the case for Liller 1 (Dalessandro et al. 2022). It is important to keep in mind that while the multipeaked MDF of Terzan 5 clearly indicates the existence of multi-iron components, it cannot be used to weight each subpopulation precisely. More stringent constraints to the sizes of the two main populations (the metal-poor population peaking at $[Fe/H]_{peak} \simeq -0.3$, generated about 12 Gyr ago, and the metal-rich population peaking at $[Fe/H]_{peak} \simeq +0.3$, formed 4.5 Gyr ago) can be derived from photometric properties. In fact, the star counts in the two detected red clumps (see Ferraro et al. 2009) led to the estimate that approximately 38% of the current stellar population of Terzan 5 (namely, $7.5 \times 10^5\ M_\odot$ of stars) originated from the youngest burst (Lanzoni et al. 2010). Regarding the relative ages of the two subpopulations, it is worth emphasizing that the analysis of the main-sequence turnoff region (Ferraro et al. 2016) has definitely removed any age-helium degeneracy (see D'Antona et al. 2010; Nataf & Gould 2012, for a thorough discussion of this problem). We use the above observational inferences to constrain the star formation history of our models.

The initial masses of newborn stars are distributed according to a Kroupa (2001) stellar initial mass function (IMF). In this work, the IMF is normalized to unity over the 0.1–100 $M_\odot$ mass range.

In some models, we also take gas outflows and/or stellar stripping into account. Energetic feedback from SNe, ram pressure and tidal stripping, in fact, may remove a large fraction of the gas that is left over from the star formation process. Clusters born in the inner Galaxy also have their low-mass stars first pushed in the outskirts by mass segregation, then peeled off by strong tidal forces, with complete dissolution of the cluster being a possible outcome (see Portegies Zwart et al. 2002).

2.2. Nucleosynthesis Prescriptions

The stellar nucleosynthesis prescriptions are at the core of any chemical evolution model. In this study, we adopt stellar yields that have been successfully tested against large chemical abundance data sets for the MW in previous work (Romano et al. 2010, 2017, 2019).

More precisely, the stellar yields are taken from Karakas (2010) for low- and intermediate-mass stars, from Doherty et al. (2014b, 2014a) for super-AGB stars, from Nomoto et al. (2013) for massive stars, and from Iwamoto et al. (1999) for type Ia SNe (SNeIa, thermonuclear explosions of white dwarfs in binary systems that completely disrupt the parent system). Stars more massive than 20 $M_\odot$ may explode as core-collapse SNe (CCSNe), releasing energies of about 10^{51} erg, or as hypernovae (HNe), releasing energies an order of magnitude higher. The HN fraction may vary (e.g., as a function of the metallicity of the system). To encompass all possible cases, we run models in which all massive stars explode as CCSNe and also models in which all stars with initial masses above 20 $M_\odot$ explode as HNe. The yield tables are linearly interpolated as a function of the initial stellar mass and metallicity and are extrapolated to the 40–100 $M_\odot$ regime (not covered by full stellar nucleosynthesis calculations in Nomoto et al. 2013) by keeping the yield constant.

While the number of CCSNe/HNe that explode in a system is plain set by the adopted star formation history and IMF, the number of expected SNIa explosions may depend on additional factors. For instance, orbital hardening and exchange interactions may lead to enhanced SNIa rates in star clusters relative to the field (Shara & Hurley 2002, 2006). In classic chemical evolution models, it is customary to assume that a constant fraction of the stellar mass in the range 3–16 $M_\odot$ enters the formation of binary systems that give rise to SNIa explosions (see, e.g., Matteucci & Recchi 2001). However, this fraction might be time and/or environment dependent. We discuss this issue in Section 3.

3. Results

In this section, we present the results of different sets of models, in which we vary in turn the mass and initial chemical composition of the gaseous clump out of which Terzan 5 emerges, the infall timescale, the number and duration of the star formation episodes, and the star formation efficiency. Since there is little doubt that the mass of Terzan 5 was higher in the past than what is observed today, $M_{stars} = (2 \pm 1) \times 10^6\ M_\odot$ (Lanzoni et al. 2010), and motivated by dynamical arguments (Baumgardt et al. 2008), we assume that the initial gas cloud mass is in the range 10^7–$10^8\ M_\odot$. We build models that produce a final stellar mass in the range 10^6–$10^7\ M_\odot$, and we study the effects of gas and stellar stripping. If stellar stripping is ineffective, the lower limit to the stellar mass range set above is consistent with the lowest value permitted by the observations (Lanzoni et al. 2010), while the upper limit allows for a high stripping efficiency.

First, we develop a series of exploratory models to qualitatively analyze the outcome of an early star formation burst that builds up the majority of the stellar populations in Terzan 5 (Sections 3.1–3.3). Then, we add the fringe star formation episode that originates the metal-rich younger stars, paying attention to quantitatively reproduce the fractions of metal-poor and metal-rich stars inferred from the red clump analysis (Section 3.4). The values of the input parameters are listed in Table 1 (Table 2) for the single-burst (double-burst) models.

3.1. A Pristine Massive Parent Cloud

We start our analysis by considering a $10^8\ M_\odot$ gas cloud with a primordial chemical composition ($Z_{in} = 0$). For the moment, we concentrate on the oldest stellar populations and forget about the young metal-rich stars. We keep the duration of the ancient (age = 12 Gyr) star formation episode that generates the old stars fixed to $\Delta t_{SF} = 1$ Gyr and vary the e-folding time in Equation (1) and the star formation efficiency in Equation (2) so as to obtain the same present-day stellar mass ($M_{stars} = 10^7\ M_\odot$) for different choices of the (τ, ν) parameter couple. The adopted values of the model parameters are reported in Table 1 (models from H01 to H08).

Clearly, the longer the infall timescale, the lower the cold gas mass available to form stars at early times and the higher the star formation efficiency required to end up with the desired total stellar mass. In Figure 1 the predictions of models from H01 through to H08 (colored lines) are compared to the observed iron distribution in Terzan 5 (gray histogram; Massari et al. 2014). The longer the infall timescale and the higher the star formation efficiency, the more the peak of the theoretical

Table 1
Model Parameters and Final Stellar Mass of the Single-burst Models

Model	$M_{\rm in}$ ($M_\odot$)	$Z_{\rm in}$	τ (Gyr)	$\Delta t_{\rm SF}$ (Gyr)	ν (Gyr^{-1})	Stripped Stars (%)	$M_{\rm stars}$ ($M_\odot$)
(1)	(2)	(3)	(4)	(5)	(6)	(7)	(8)
H01	10^8	0	0.5	1.0	0.27	0	10^7
H02	10^8	0	1.0	1.0	0.31	0	10^7
H03	10^8	0	2.0	1.0	0.44	0	10^7
H04	10^8	0	3.0	1.0	0.59	0	10^7
H05	10^8	0	4.0	1.0	0.74	0	10^7
H06	10^8	0	5.0	1.0	0.89	0	10^7
H07	10^8	0	6.0	1.0	1.03	0	10^7
H08	10^8	0	7.0	1.0	1.16	0	10^7
H08s	10^8	0	7.0	1.0	1.16	56	4.4×10^6
L01	10^7	0.005	0.5	1.0	0.27	0	10^6
L02	10^7	0.005	1.0	1.0	0.31	0	10^6
L03	10^7	0.005	2.0	1.0	0.44	0	10^6
L04	10^7	0.005	3.0	1.0	0.59	0	10^6
L05	10^7	0.005	4.0	1.0	0.74	0	10^6
L06	10^7	0.005	5.0	1.0	0.89	0	10^6
L06s	10^7	0.005	5.0	1.0	0.89	47	5.3×10^5
L07	10^7	0.005	6.0	1.0	1.03	0	10^6
L08	10^7	0.005	7.0	1.0	1.16	0	10^6
T01	10^7	0.005	5.0	0.1	10.0	0	10^6
T01s	10^7	0.005	5.0	0.1	10.0	67	3.3×10^5
T02	10^7	0.005	5.0	0.5	1.81	0	10^6
T03	10^7	0.005	5.0	2.0	0.43	0	10^6
T04	10^7	0.005	7.0	0.1	14.2	0	10^6
T04s	10^7	0.005	7.0	0.1	14.2	52	4.8×10^5

Note. This includes (1) model name, (2) total initial mass, and (3) metallicity of the infalling gas, (4) infall timescale, (5) duration of the star formation, (6) star formation efficiency, (7) percentage of stripped stars (if any), and (8) present-day stellar mass of the system.

MDF is skewed toward high metallicities, in better agreement with the observations.

We face, unsurprisingly, the well-known problem commonly referred to as the "G-dwarf problem", namely, a predicted excess of low-metallicity stars in systems that evolve as a closed box (van den Bergh 1962; Pagel & Patchett 1975; Martinelli & Matteucci 2000; Greener et al. 2021). It is obvious that Terzan 5 does not evolve as an isolated system. Instead, its evolution is strongly influenced by the surroundings. In fact, a better fit to the observed MDF of Terzan 5 is obtained not only by assuming a somewhat inefficient gas cooling ($\tau = 7$ Gyr for models H08 and H08s versus $\tau = 0.5$ Gyr for model H01), possibly dictated by lively star formation activity in neighboring areas that keeps the gas warm, but also by accounting for the loss of a significant fraction of metal-poor stars due to mass segregation and tidal stripping[9] (model H08s). The purple shaded area in Figure 1 that fits the data best in fact refers to a situation in which 75% of the stars with [Fe/H] < -0.4 have been stripped, corresponding to a 56% reduction of the total stellar mass. This leaves us with $M_{\rm stars} \simeq 4.4 \times 10^6\ M_\odot$ at present, which is hardly compatible with the observed value for the old stellar component of Terzan 5 within the quoted uncertainty.

Figure 2 shows the behavior of the abundance ratios of Al, Mg, Si, and Ca to Fe as a function of metallicity predicted by model H08s. The lower (upper) envelope of the shaded area in each panel refers to the case in which HN nucleosynthesis is (is not) included, with all (no) stars above $20\,M_\odot$ exploding as HNe. The shaded area stands for intermediate figures. The agreement among model predictions and observations is satisfactory,[10] also taking into account the many uncertainties that still affect the stellar nucleosynthesis prescriptions (Romano et al. 2010).

3.2. A Pre-enriched Low-mass Gas Cocoon

In this section, we discuss the results of a set of models (Table 1, models from L01 to L08) that share the same parameter values with the previous set of models, bar the total amount ($M_{\rm in} = 10^7\ M_\odot$) and initial chemical composition ($Z_{\rm in} = 0.005$) of the gas. The final stellar mass is $M_{\rm stars} = 10^6\ M_\odot$, and no synthetic stars are created below [Fe/H] $= -1$ by construction.

Similarly to what we have seen in the previous section, the theoretical MDF matches the observed MDF more closely if (i) the gas is kept warm (due to strong stellar feedback in the surroundings?), so that the cold gas that fuels the star formation is accreted on long timescales and (ii) the system is deprived of a non-negligible fraction (here, 65%) of its long-lived low-mass stars with [Fe/H] $\leqslant -0.4$ dex (Figure 3). After stripping,

[9] It is reasonable to expect that as the star formation and the chemical enrichment proceed, cooling flows bring the enriched gas to the cluster center. Therefore, metal-rich stars form in the inner regions, while metal-poor stars are mainly found in the outer regions. For these reasons, metal-poor low-mass stars are more susceptible to stripping.

[10] We recall that the metal-rich subpopulation is not reproduced by this model by construction.

Table 2
Model Parameters and Final Stellar Mass of the Double-burst Models

Model	$M_{\rm in}$ ($M_\odot$)	$Z_{\rm in}$	τ (Gyr)	$\Delta t_{SF_{\rm I}}$ (Gyr)	$\Delta t_{SF_{\rm II}}$ (Gyr)	$\nu_{\rm I}$ (Gyr^{-1})	$\nu_{\rm II}$ (Gyr^{-1})	Stripped Stars (%)	Gas Loss	SNIa Precursors Retention	$M_{\rm stars\ I}$ ($M_\odot$)	$M_{\rm stars\ II}$ ($M_\odot$)
(1)	(2)	(3)	(4)	(5)	(6)	(7)	(8)	(9)	(10)	(11)	(12)	(13)
S01s	4×10^7	0.005	5.0	0.1	0.1	10.0	10.0	41	no	yes	1.3×10^6	3.0×10^6
S02s	4×10^7	0.005	5.0	0.1	0.1	10.0	10.0	58	yes	yes	1.3×10^6	7.5×10^5
S03s	4×10^7	0.005	5.0	0.1	0.1	10.0	10.0	58	yes	no	1.3×10^6	7.5×10^5

Note. This includes (1) model name, (2) total initial mass and (3) metallicity of the infalling gas, (4) infall timescale, (5) duration of the early and (6) late star formation episodes, (7) star formation efficiency of the first and (8) second star formation episode, (9) percentage of stripped stars (if any), (10) a flag that indicates if gas outflow/stripping is taken into account, (11) a flag that indicates whether SNIa progenitors are retained, and (12) the present-day stellar mass assembled in the first and (13) in the second starburst (their sum gives the current total mass of the system).

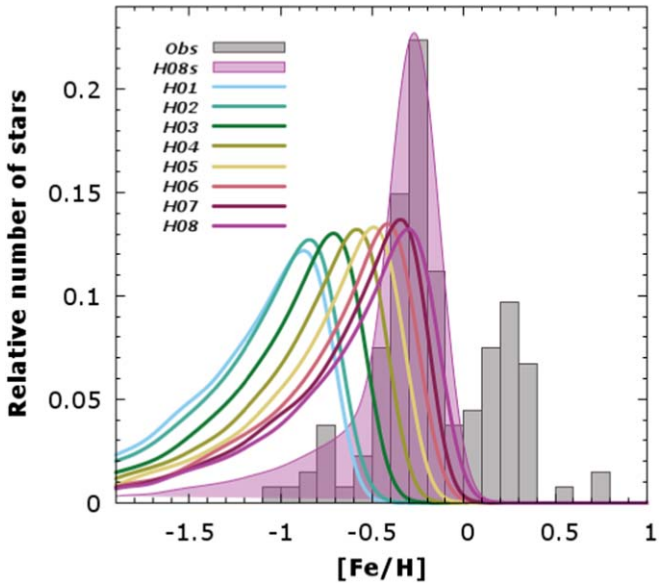

Figure 1. Observed (gray histogram; Massari et al. 2014) and predicted (solid lines and shaded area) iron distributions of the stellar populations of Terzan 5. The theoretical distributions are convolved with a Gaussian with a dispersion of $\sigma = 0.1$ dex in order to take the observational errors into account. The shaded area refers to model H08s, which also takes the stripping of low-metallicity stars into account (see text).

model L06s ends with a total present-day stellar mass of $\sim 5.3 \times 10^5$ $M_\odot$, which is marginally compatible with the observational estimate (when also taking into account the increase in stellar mass that is expected as a consequence of the second late star formation burst). The chemical properties of the subsolar populations of Terzan 5 are well reproduced by model L06s (Figure 4), which also matches the position of the main peak of the MDF well.

We note that starting from a slightly pre-enriched gas favors the appearance of a secondary metal-poor MDF peak. This conclusion is totally unrelated to the assumed mass of the progenitor. What matters, in fact, are the relative proportions between the mass of the cold gas entering the star-forming regions (dictated by the choice of τ) and the mass of the stars born in the system (dictated by the choice of ν) at each time, and not their absolute values.

While our chemical evolution model cannot place stringent constraints on the initial mass of the progenitor of Terzan 5 (although values as high as $M_{\rm in} = 10^8$ $M_\odot$ seem somewhat disfavored), it is pretty much consistent with the expectations from dynamical investigations. Baumgardt et al. (2008) suggest that gas clouds with masses in excess of 10^7 $M_\odot$ tend to retain their gas despite multiple SN events, which would explain the self-enrichment of the most massive clusters. However, it is worth emphasizing that these models are tailored to systems evolving in a much less dense environment than the one provided by the inner Galaxy in its infancy.

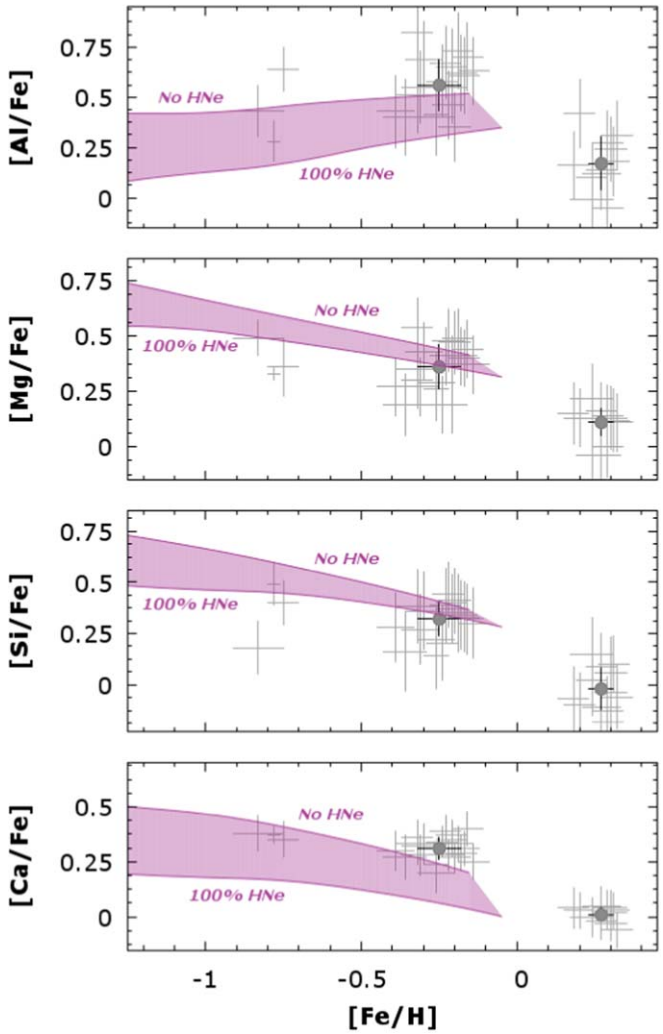

Figure 2. *From top to bottom:* runs of [Al/Fe], [Mg/Fe], [Si/Fe], and [Ca/Fe] as functions of [Fe/H] in Terzan 5 predicted by model H08s, taking into account the uncertainties due to the fraction of stars that explode as HNe (shaded areas). Data for individual giants (crosses), along with average values for the different components (circles), with the exception of the metal-poor regime, where the sample amounts to only three objects, are from Origlia et al. (2011, 2013). Theoretical and observed abundance ratios are normalized to the solar values by Magg et al. (2022).

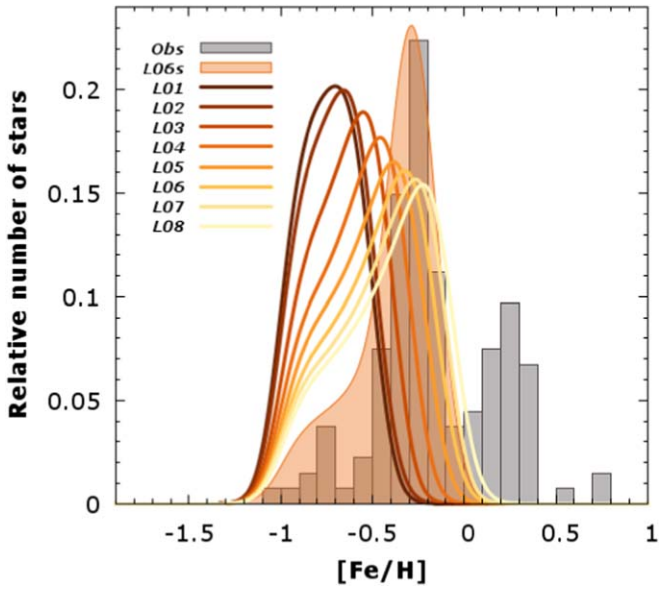

Figure 3. Same as Figure 1, but for models from L01 through to L08 (solid lines). The shaded area refers to model L06s, allowing for stellar stripping.

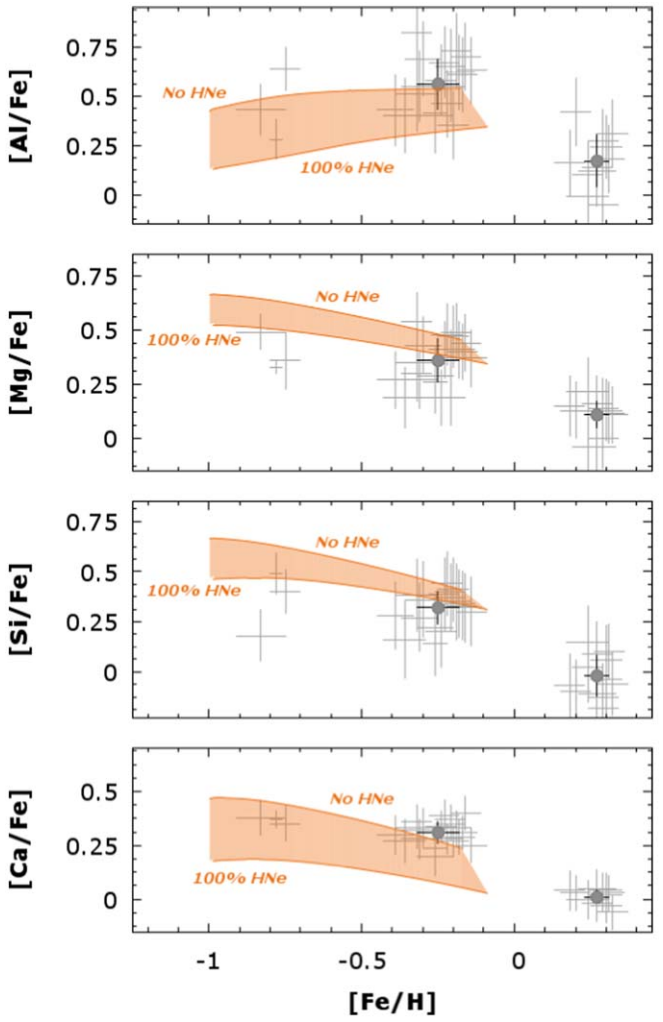

Figure 4. Same as Figure 2, but for model L06s.

3.3. Duration of the First Star Formation Episode

The analysis of the CMD of Terzan 5 allows an estimate of the ages of its stellar populations. Ferraro et al. (2016) find that the subsolar components are consistent with ages of 12 ± 1 Gyr. This means that the duration of the star formation episode that formed the oldest stars in Terzan 5 is $\Delta t_{\rm SF} \leqslant 2$ Gyr. In principle, it could be as short as few tens of million years. The models discussed in the previous sections assume a fiducial value of $\Delta t_{\rm SF} = 1$ Gyr. In this section, we examine the effects of $\Delta t_{\rm SF}$ variations from 100 Myr to 2 Gyr (see Table 1, models T01–T04).

Figure 5 illustrates the changes in the shape of the predicted MDF produced by variations in the duration of the main star formation episode compatible with the observed CMD (solid purple lines of progressively lighter shade for progressively longer star formation episodes). Since all the models have to produce the same final stellar mass, the shorter $\Delta t_{\rm SF}$, the higher the required star formation efficiency (Table 1). A higher star formation rate at early times (model T01, darkest purple line) results in a more pronounced secondary peak at $[{\rm Fe/H}] \simeq -0.8$, while this feature completely disappears when the star formation lasts longer than 1 Gyr (model T03, lightest purple line). On the other hand, the position of the main peak does not change much with changing $\Delta t_{\rm SF}$—it is rather dictated by the adopted value of τ (compare models T01 and T04, assuming $\tau = 5$ and 7 Gyr, respectively). Not differently from what has been found previously, a better agreement with the observed MDF of Terzan 5 is obtained by imposing that stellar stripping removed the majority of the low-mass metal-poor stars (80% of all stars below $[{\rm Fe/H}] = -0.4$, models T01s and T04s, shaded areas in Figure 5).

In principle, the duration of the star formation activity also affects the predicted trend of the elemental abundance ratios as a function of [Fe/H]. The longer $\Delta t_{\rm SF}$, in fact, the larger the amount of iron restored by SNeIa on long timescales that enters the formation of subsequent stellar generations, resulting in a prominent reduction of several element-to-iron abundance ratios at high metallicities (especially for the elements that are produced for the most part by massive stars). However, the request that the final stellar mass be the same for all models translates into the demand for greater star formation efficiencies when the star formation lasts for less time. This leads to a larger production of Fe from massive stars on short timescales in the models with quicker bursts, which accompanies the enhanced fast making of all other massive star products. The net result is that different models reach similar final metallicities, while the element-to-iron ratios differences amount to 0.2 dex at most. The most effective litmus test of the duration of the star formation burst is thus the observed MDF of the system.

3.4. The Two-burst Models

The subsolar metallicity components of Terzan 5 have chemical properties consistent with being born on a relatively short timescale ($\Delta t_{SF_{\rm I}} = 100$ Myr) from a slightly metal-enriched gas cocoon significantly more massive (with a mass of a few $10^7\,M_{\odot}$) than the present system. In order to reproduce the chemical properties of the youngest (age =4.5 Gyr) population of Terzan 5 that accounts for a non-negligible fraction (38%; Lanzoni et al. 2010) of the present-day total mass of the cluster, we suggest a second short ($\Delta t_{SF_{\rm II}} = 100$ Myr) star formation

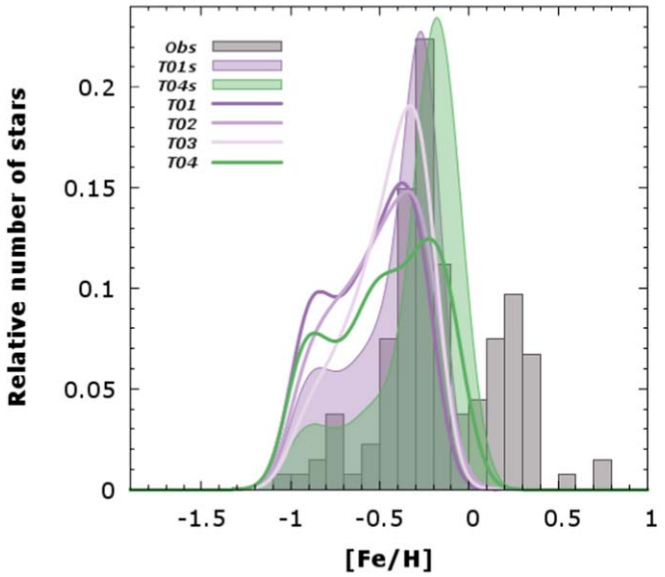

Figure 5. Same as Figure 1, but for models from T01 through to T04 (solid lines). The shaded areas refer to models including stellar stripping (T01s and T04s).

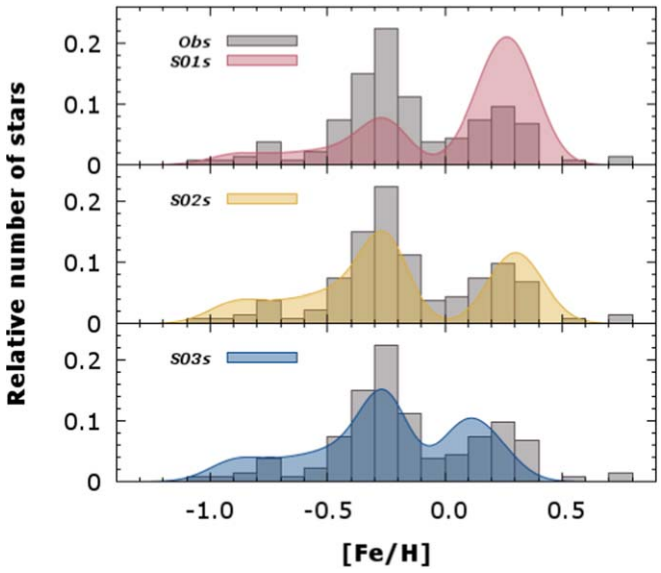

Figure 6. Observed (gray histogram; Massari et al. 2014) and predicted (shaded areas) iron distributions of the stellar subpopulations of Terzan 5. The theoretical distributions are convolved with a Gaussian of dispersion $\sigma = 0.1$ dex in order to take the observational errors into account.

episode after a long (7.5 Gyr) interlude in which stars are basically not formed, as inferred from CMD analyses. Hereinafter, we use the I/II subscript when referring to the first/second star formation episode. Note that our models give no clues about the physical reasons for this long quiescent phase, and that a very low-level star formation activity in between the two main events (similar to what is inferred for Liller 1; Dalessandro et al. 2022) could still be accommodated, with no major impact on the model results. In future work, we will make use of hydrodynamical simulations (Calura et al. 2019; Lacchin et al. 2021) to study the formation of the young stellar populations in more detail.

We start from a configuration that reproduces the chemical properties of the oldest stars of Terzan 5. Model T01s offers a good starting point (see the previous section), but it leaves behind only 3.3×10^5 $M_\odot$ of stars (see Table 1, row 20), which is too low compared to the current total mass of Terzan 5, namely, $M_{\rm stars} = (2 \pm 1) \times 10^6$ $M_\odot$ (Lanzoni et al. 2010). Thus, we consider a four times more massive progenitor, $M_{\rm in} = 4 \times 10^7$ $M_\odot$, yielding a present-day mass $M_{\rm stars\ I} = 1.3 \times 10^6$ $M_\odot$[11] for the subsolar metallicity component, in excellent agreement with the empirical mass estimate of Lanzoni et al. (2010).

We thus explore three models, namely S01s, S02s, and S03s, that have the same star formation parameters, but differ in the amount of gas losses/stellar stripping and in the possibility or inability of preferentially retaining SNIa progenitors, as shown in Table 2.

In model S01s (see Table 2 and the shaded red area in Figure 6, upper panel), the young stars form with the same efficiency of the conversion of gas into stars as the old stars (50%), without any gas loss from the system. The young population therefore dominates the total mass budget, which is at variance with the empirical mass estimates.

At odds with the previous model, model S02s allows gas losses (see Table 2). The removal of a major fraction of the gas left over from the first star formation episode yields the right proportions of young to old stars, as shown in the last two columns of Table 2 (see also the shaded yellow area in the middle panel of Figure 6). It is worth emphasizing that in model S02s and in model S01s, the white dwarfs leading to SNIa explosions that form during the first star formation burst are not lost from the system, but settle in the central regions of the protocluster, so that the SNIa rate is boosted in the inner star-forming regions. Therefore, the youngest stars that are generated in the center reflect the Fe-enriched composition of a medium polluted by all these SNeIa. This reproduces the observed trends of [Al/Fe], [Mg/Fe], [Si/Fe], and [Ca/Fe] versus [Fe/H] of both the subsolar and the metal-rich populations well (see Figure 7).

Model S03s assumes that most (80%) of the SNIa precursors are lost together with the low-mass low-metallicity single stars (Table 2). Although the model predictions are still compatible with the observed MDF (shaded blue area in Figure 6), they fail to reproduce the observed low [Al/Fe] and [α/Fe] ratios of the metal-rich component (upper blue line in all panels of Figure 7).

Hence, this analysis shows that gas loss and the retention of a major fraction of Fe produced by SNeIa are fundamental ingredients for reproducing both the MDF and the abundance ratios of the metal-rich population in Terzan 5. As a result, only model S02s succeeds in predicting all the observational constraints simultaneously (mass of the two main populations, MDF, and abundance ratios).

4. Discussion and Conclusions

Terzan 5 is a complex stellar system located in the outskirts of the inner bulge and characterized by peculiar features that clearly distinguish it from a typical globular cluster. It harbors at least three subpopulations with distinct ages and chemical properties (Ferraro et al. 2016, and references therein) and the largest population of millisecond pulsars hitherto identified in the MW (Ransom et al. 2005; Cadelano et al. 2018; Martsen et al. 2022). All these characteristics are readily accounted for if

[11] This value takes into account stripping of 80% of the long-lived stars with [Fe/H] < -0.4, which allows a better fit to the observed MDF in the low-metallicity regime.

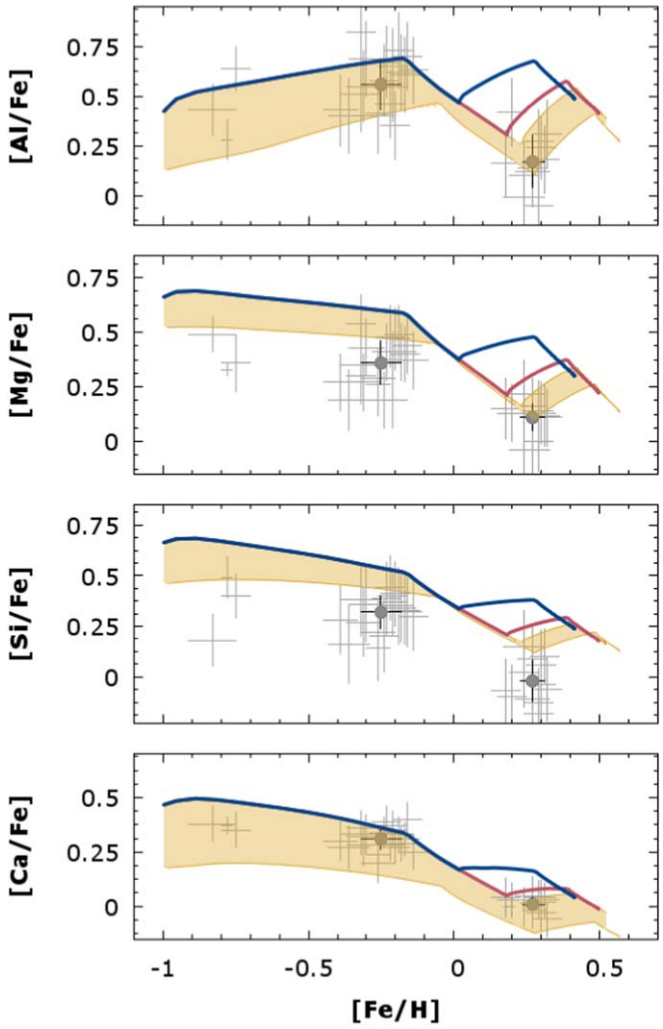

Figure 7. *From top to bottom:* [Al/Fe], [Mg/Fe], [Si/Fe], and [Ca/Fe] vs. [Fe/H] in Terzan 5 predicted by the models shown in Figure 6 (same color-coding). The shaded areas represent the uncertainties related to the assumed HN fraction (only for model S02s). Data are from Origlia et al. (2011, 2013). All abundance ratios are normalized assuming the chemical composition of the Sun recommended by Magg et al. (2022).

Terzan 5 is the compact remnant of a more massive system that self-enriched before losing most of its initial mass.

Alternative scenarios have been proposed in the literature. The hypothesis of a dwarf galaxy progenitor can be rejected straight away for several reasons. First, the orbit of Terzan 5 clearly points to an object that formed in situ (Massari et al. 2015, 2019; Baumgardt et al. 2019; Callingham et al. 2022). Second, the location in the age–metallicity space of its main stellar population perfectly matches the trend followed by in situ systems (at $[Fe/H] \sim -0.3$, ex situ objects are more than 2 Gyr younger; see, e.g., Massari et al. 2019; Kruijssen et al. 2019). Finally, it is important to keep in mind that the extreme metallicity regime observed for the two main subpopulations of Terzan 5 is characteristic of the MW bulge environment, while it is clearly incompatible with the iron abundance of any known dwarf galaxy in the local Universe.

Matsui et al. (2019) investigated the formation and evolution of young massive clusters during major galaxy mergers. These authors find that several clusters distribute within a few kiloparsec from the center of the merger remnant (see their Figure 4) and that the cluster mass function has an excess around $10^7\,M_\odot$ (see their Figure 6).[12] Some of the clusters in the simulations of Matsui et al. (Matsui et al. 2019) have multi-aged populations that originate from gas capture when the clusters pass through dense gas regions. However, the models of Matsui et al. (2019) predict just a mild metallicity enhancement that is certainly not able to reproduce the supersolar population of Terzan 5, likely due to the short time that elapses between the main bursts and/or to the neglection of SNeIa. In fact, their second-generation stars are enriched by SNeII alone, while the chemical patterns observed in Terzan 5 (Origlia et al. 2011) clearly demonstrate that the metal-rich component has been enriched by both type II and type Ia SNe.

The possibility that Terzan 5 originated in the collision between a GC and a giant molecular cloud of appropriate metallicity has been suggested by several authors (McKenzie & Bekki 2018; Bastian & Pfeffer 2022). As discussed by the authors themselves, events like this are extremely rare because they require highly fine-tuned combinations of events. However, the increasing number of discovered objects similar to Terzan 5 (Ferraro et al. 2021) and the evidence in favor of prolonged star formation histories or more than two star formation bursts (Dalessandro et al. 2022; C. Crociati et al. 2023, in preparation) make these scenarios less likely.

Instead, it is possible that Terzan 5 is the relic of a gaseous clump that originated from the fragmentation of an early disk. Bulges of disk galaxies are known to take their shapes through varied (and not mutually exclusive) formation mechanisms, and the coalescence of subsystems originating from the fragments of an early unstable disk is one possibility (e.g., Elmegreen et al. 2008). Strong radiative stellar feedback can disperse even the most massive clumps after they turn 5–20% of their mass into stars on a timescale of 10–100 Myr, but the stars might remain bound (Hopkins et al. 2012; see also Mandelker et al. 2017).

In this work, we explored a set of chemical evolution models aimed at reproducing the mass, metallicity distribution function (MDF), and chemical abundance patterns measured so far in Terzan 5 under the assumption that it was the product of the self-enrichment process of one of those primordial gas clumps that could have contributed to the formation of the Galactic bulge at the epoch of the MW bulge assembly. The model that best reproduces the observations is model S02s, which rests on a number of assumptions that will be explored in detail in future work focusing on the dynamical aspects. We summarize our current findings as follows.

1. Of all the explored models, model S02s in Table 2 can reasonably account for all the observables, namely, mass, MDF, and abundance ratios of both the old metal-poor and the young metal-rich subpopulations.
2. The relative weights of the metal-poor and metal-rich subpopulations of Terzan 5 (comprising about 62% and 38% of the current mass of the cluster, respectively) are explained by assuming that Terzan 5 formed via two main star formation episodes separated by a long period (7.5 Gyr) of quiescence or low-level star formation activity, in agreement with CMD analyses. It remains to be seen if delayed energy release from SNeIa allows that

[12] In this respect, it would be interesting to investigate in simulations if the accretion of the Heracles satellite (Horta et al. 2021) could have triggered the formation of massive clusters in the MW bulge as well.

some gas is kept warm while it is still trapped in the potential well of the system for later star formation.

3. The oldest stars (ages $\simeq$12 Gyr) are formed from a gas clump with a mass of a few $10^7\,M_{\odot}$. According to our simulations, if the gas clump has a slightly pre-enriched ($Z \simeq 0.005$) chemical composition, a secondary more metal-poor peak in the MDF is more easily produced.
4. After its formation, the proto-Terzan 5 should lose a large fraction (>50%) of its metal-poor low-mass stars (owing to mass segregation and tidal stripping) as well as most of the gas left over from the first star formation episode (owing to the combined effects of SN feedback, ram pressure, and tidal stripping). In order to explain the chemical properties of the second-generation stars, it is crucial to incorporate a detailed treatment of the ejecta of the first stellar generations in the calculations.
5. In particular, the white dwarfs formed during the first star formation burst should settle at the center of the cluster and escape stripping, so that the rate of SNIa explosions is enhanced and Fe production maximized there. This is a necessary condition to reproduce the high-metallicity peak of the MDF and the observed abundance ratios of the metal-rich subpopulations. If this were not the case, the recent star formation burst would tend to restore the abundance ratios to values more typical of massive star ejecta, in disagreement with the observations (see the blue lines in Figure 7).
6. To produce the right proportion of young stars, we need to mix the ejecta of older stellar generations into a fraction of ambient gas. Our model cannot discriminate whether this gas comes from cooling of warm gas surrounding the protocluster (see the second item above) or if it is collected through interactions with a giant molecular cloud. Hydrodynamical simulations (Pflamm-Altenburg & Kroupa 2009; McKenzie & Bekki 2018; Matsui et al. 2019) have shown that, in principle, the latter is a viable hypothesis (but see the above discussion). In future work, we will couple the passive evolution of the oldest stellar populations of Terzan 5 with gas accretion via bound cluster-cloud collisions to self-consistently study the rejuvenation of the cluster by means of high-resolution 3D hydrodynamical simulations (Calura et al. 2019; Lacchin et al. 2021).

Finally, we use our most representative two-burst model to make a prediction of the expected He abundance distribution. Model S02s (see Section 3.4, Table 2, and Figures 6–7) returns a wide He abundance distribution, ranging from $Y \simeq 0.26$ for the oldest stars to $Y \simeq 0.335$ for the youngest stars, with a main peak at $Y = 0.29$ and two local maxima at $Y = 0.26$ and $Y \simeq 0.335$ (see Figure 8). This model, like all the others discussed in this paper, starts from a primordial He abundance $Y_{\rm P} = 0.248$, consistent with the standard model primordial value and with the abundance measured in near-pristine intergalactic gas (see Cooke & Fumagalli 2018, and references therein). Note that normally, stellar isochrones such as those used by Ferraro et al. (2016) or by Bensby et al. (2013) in studying the populations of giants and microlensed dwarfs/subgiant bulge stars, respectively, adopt a primordial value of $Y_{\rm P} \simeq 0.24$. Isochrone fitting of the double turnoff in Terzan 5 (Ferraro et al. 2016) returns an old age of 12 Gyr, adopting a helium mass fraction $Y = 0.26$, for the dominant metal-poor component and an intermediate age of 4.5 Gyr, adopting

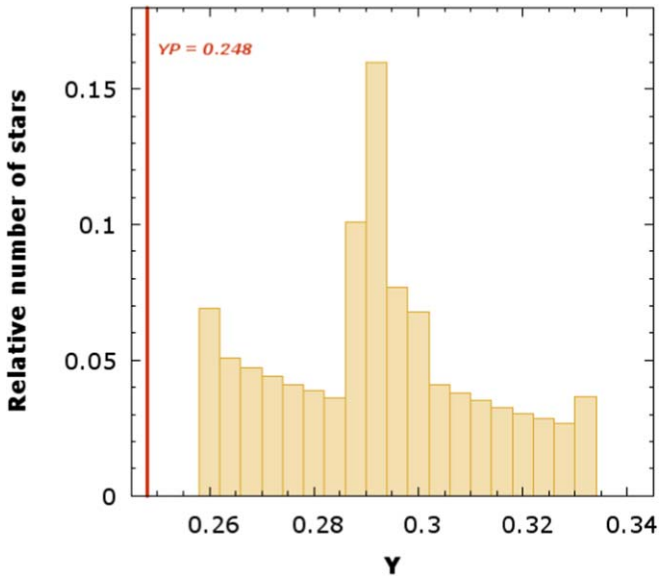

Figure 8. Helium distribution of the stellar populations of Terzan 5 after model S02s. The vertical red line indicates the primordial He abundance adopted by our chemical evolution models.

$Y = 0.29$, for the centrally concentrated supersolar metallicity component.

If Terzan 5 is helium enhanced, as we predict, it will require the development of ad hoc isochrones and stellar model atmospheres. Moreover, a self-consistent evaluation of the chemical enrichment of proto-Terzan 5 would require the use of stellar yields computed specifically for He-enhanced stars. Unfortunately, the advanced evolution, chemical yields, and final fates of He-rich stars have so far been explored in only limited ranges of initial stellar mass and metallicity (Shingles et al. 2015; Althaus et al. 2017).

Another potential problem affecting the yields and thus the chemical evolution model predictions is the neglect of the effects of binary interactions among massive stars, which may be particularly relevant in the high-density environment of proto-Terzan 5. Investigations of the effects of stellar multiplicity on massive star yields are still very limited, but promising studies are ongoing (Farmer et al. 2021; Farmer et al. 2023).

Acknowledgments

We dedicate this paper to the memory of our colleague and friend, Antonio Luigi Sollima, who sadly passed away earlier this year. We are grateful to the anonymous referee for the constructive feedback on the manuscript. This research was supported by the Munich Institute for Astro, Particle and BioPhysics (MIAPbP) which is funded by the Deutsche Forschungsgemeinschaft (DFG, German Research Foundation) under Germany's Excellence Strategy EXC-2094 390783311. This research is part of the project *Cosmic-Lab* at the Physics and Astronomy Department of the University of Bologna (http://www.cosmic-lab.eu/Cosmic-Lab/Home.html). This research has been funded by project *Light-on-Dark*, granted by the Italian MIUR through contract PRIN-2017K7REXT (PI: F. R. Ferraro). The figures in this article use color-blind friendly palettes retrieved from Paul Tol's website (https://personal.sron.nl/~pault/#fig:scheme_rainbow_discrete).

ORCID iDs

Donatella Romano https://orcid.org/0000-0002-0845-6171
Francesco R. Ferraro https://orcid.org/0000-0002-2165-8528
Livia Origlia https://orcid.org/0000-0002-6040-5849
Simon Portegies Zwart https://orcid.org/0000-0001-5839-0302
Barbara Lanzoni https://orcid.org/0000-0001-5613-4938
Chiara Crociati https://orcid.org/0009-0002-8571-5170
Davide Massari https://orcid.org/0000-0001-8892-4301
Emanuele Dalessandro https://orcid.org/0000-0003-4237-4601
Alessio Mucciarelli https://orcid.org/0000-0001-9158-8580
R. Michael Rich https://orcid.org/0000-0003-0427-8387
Francesco Calura https://orcid.org/0000-0002-6175-0871
Francesca Matteucci https://orcid.org/0000-0001-7067-2302

References

Althaus, L. G., De Gerónimo, F., Córsico, A., Torres, S., & García-Berro, E. 2017, A&A, 597, A67
Athanassoula, E. 2005, in AIP Conf. Ser. 804, Planetary Nebulae as Astronomical Tools, ed. R. Szczerba, G. Stasińska, & S. K. Gorny (Melville, NY: AIP), 333
Athanassoula, E., Rodionov, S. A., & Prantzos, N. 2017, MNRAS, 467, L46
Baade, W. 1946, PASP, 58, 249
Babusiaux, C. 2016, PASA, 33, e026
Barbuy, B., Chiappini, C., & Gerhard, O. 2018, ARA&A, 56, 223
Bastian, N., & Pfeffer, J. 2022, MNRAS, 509, 614
Baumgardt, H., Hilker, M., Sollima, A., & Bellini, A. 2019, MNRAS, 482, 5138
Baumgardt, H., Kroupa, P., & Parmentier, G. 2008, MNRAS, 384, 1231
Baumgardt, H., & Makino, J. 2003, MNRAS, 340, 227
Bekki, K., & Freeman, K. C. 2003, MNRAS, 346, L11
Bensby, T., Adén, D., Meléndez, J., et al. 2011, A&A, 533, A134
Bensby, T., Feltzing, S., Gould, A., et al. 2017, A&A, 605, A89
Bensby, T., Yee, J. C., Feltzing, S., et al. 2013, A&A, 549, A147
Bica, E., Ortolani, S., & Barbuy, B. 2016, PASA, 33, e028
Bournaud, F., Daddi, E., Elmegreen, B. G., et al. 2008, A&A, 486, 741
Cadelano, M., Ransom, S. M., Freire, P. C. C., et al. 2018, ApJ, 855, 125
Callingham, T. M., Cautun, M., Deason, A. J., et al. 2022, MNRAS, 513, 4107
Calura, F., D'Ercole, A., Vesperini, E., Vanzella, E., & Sollima, A. 2019, MNRAS, 489, 3269
Catchpole, R. M., Whitelock, P. A., Feast, M. W., et al. 2016, MNRAS, 455, 2216
Clarkson, W., Sahu, K., Anderson, J., et al. 2008, ApJ, 684, 1110
Combes, F., Debbasch, F., Friedli, D., & Pfenniger, D. 1990, A&A, 233, 82
Cooke, R. J., & Fumagalli, M. 2018, NatAs, 2, 957
Crociati, C., Valenti, E., Ferraro, F. R., et al. 2023, ApJ, in press (arXiv:2305.04595)
Dalessandro, E., Crociati, C., Cignoni, M., et al. 2022, ApJ, 940, 170
D'Antona, F., Ventura, P., Caloi, V., et al. 2010, ApJL, 715, L63
Doherty, C. L., Gil-Pons, P., Lau, H. H. B., et al. 2014a, MNRAS, 441, 582
Doherty, C. L., Gil-Pons, P., Lau, H. H. B., Lattanzio, J. C., & Siess, L. 2014b, MNRAS, 437, 195
Eggen, O. J., Lynden-Bell, D., & Sandage, A. R. 1962, ApJ, 136, 748
Elmegreen, B. G., Bournaud, F., & Elmegreen, D. M. 2008, ApJ, 688, 67
Farmer, R., Laplace, E., de Mink, S. E., & Justham, S. 2021, ApJ, 923, 214
Farmer, R., Laplace, E., Ma, J.-Z., de Mink, S. E., & Justham, S. 2023, ApJ, 948, 111
Ferraro, F. R., Dalessandro, E., Mucciarelli, A., et al. 2009, Natur, 462, 483
Ferraro, F. R., Massari, D., Dalessandro, E., et al. 2016, ApJ, 828, 75
Ferraro, F. R., Pallanca, C., Lanzoni, B., et al. 2021, NatAs, 5, 311
Gonzalez, O. A., Rejkuba, M., Zoccali, M., et al. 2012, A&A, 543, A13
Gonzalez, O. A., Zoccali, M., Vasquez, S., et al. 2015, A&A, 584, A46
Gratton, R., Bragaglia, A., Carretta, E., et al. 2019, A&ARv, 27, 8
Greener, M. J., Merrifield, M., Aragón-Salamanca, A., et al. 2021, MNRAS, 502, L95
Hasselquist, S., Zasowski, G., Feuillet, D. K., et al. 2020, ApJ, 901, 109
Haywood, M., Di Matteo, P., Snaith, O., & Calamida, A. 2016, A&A, 593, A82
Hill, V., Lecureur, A., Gómez, A., et al. 2011, A&A, 534, A80
Hopkins, P. F., Kereš, D., Murray, N., Quataert, E., & Hernquist, L. 2012, MNRAS, 427, 968
Horta, D., Schiavon, R. P., Mackereth, J. T., et al. 2021, MNRAS, 500, 1385
Howes, L. M., Casey, A. R., Asplund, M., et al. 2015, Natur, 527, 484
Immeli, A., Samland, M., Gerhard, O., & Westera, P. 2004, A&A, 413, 547
Iwamoto, K., Brachwitz, F., Nomoto, K., et al. 1999, ApJS, 125, 439
Karakas, A. I. 2010, MNRAS, 403, 1413
Kennicutt, R. C. J. 1998, ApJ, 498, 541
Kormendy, J., & Kennicutt, R. C. J. 2004, ARA&A, 42, 603
Kroupa, P. 2001, MNRAS, 322, 231
Kruijssen, J. M. D., Pfeffer, J. L., Reina-Campos, M., Crain, R. A., & Bastian, N. 2019, MNRAS, 486, 3180
Lacchin, E., Calura, F., & Vesperini, E. 2021, MNRAS, 506, 5951
Lanzoni, B., Ferraro, F. R., Dalessandro, E., et al. 2010, ApJ, 717, 653
Magg, E., Bergemann, M., Serenelli, A., et al. 2022, A&A, 661, A140
Mandelker, N., Dekel, A., Ceverino, D., et al. 2017, MNRAS, 464, 635
Martinelli, A., & Matteucci, F. 2000, A&A, 353, 269
Martsen, A. R., Ransom, S. M., DeCesar, M. E., et al. 2022, ApJ, 941, 22
Massari, D., Dalessandro, E., Ferraro, F. R., et al. 2015, ApJ, 810, 69
Massari, D., Koppelman, H. H., & Helmi, A. 2019, A&A, 630, L4
Massari, D., Mucciarelli, A., Ferraro, F. R., et al. 2014, ApJ, 795, 22
Matsui, H., Tanikawa, A., & Saitoh, T. R. 2019, PASJ, 71, 19
Matteucci, F. 2012, Chemical Evolution of Galaxies (Berlin: Springer)
Matteucci, F. 2021, A&ARv, 29, 5
Matteucci, F., & Recchi, S. 2001, ApJ, 558, 351
McKenzie, M., & Bekki, K. 2018, MNRAS, 479, 3126
Minniti, D., Fernández-Trincado, J. G., Ripepi, V., et al. 2018, ApJL, 869, L10
Nataf, D. M., & Gould, A. P. 2012, ApJL, 751, L39
Nieuwmunster, N., Nandakumar, G., Spitoni, E., et al. 2023, A&A, 671, A94
Nogueras-Lara, F., Schödel, R., & Neumayer, N. 2021, A&A, 653, A133
Nomoto, K., Kobayashi, C., & Tominaga, N. 2013, ARA&A, 51, 457
Origlia, L., Massari, D., Rich, R. M., et al. 2013, ApJL, 779, L5
Origlia, L., Mucciarelli, A., Fiorentino, G., et al. 2019, ApJ, 871, 114
Origlia, L., Rich, R. M., Ferraro, F. R., et al. 2011, ApJL, 726, L20
Ortolani, S., Renzini, A., Gilmozzi, R., et al. 1995, Natur, 377, 701
Pagel, B. E. J., & Patchett, B. E. 1975, MNRAS, 172, 13
Pflamm-Altenburg, J., & Kroupa, P. 2009, MNRAS, 397, 488
Portegies Zwart, S. F., Makino, J., McMillan, S. L. W., & Hut, P. 2002, ApJ, 565, 265
Queiroz, A. B. A., Chiappini, C., Perez-Villegas, A., et al. 2021, A&A, 656, A156
Ransom, S. M., Hessels, J. W. T., Stairs, I. H., et al. 2005, Sci, 307, 892
Renzini, A., Gennaro, M., Zoccali, M., et al. 2018, ApJ, 863, 16
Rich, R. M., Johnson, C. I., Young, M., et al. 2020, MNRAS, 499, 2340
Rojas-Arriagada, A., Recio-Blanco, A., Hill, V., et al. 2014, A&A, 569, A103
Rojas-Arriagada, A., Zasowski, G., Schultheis, M., et al. 2020, MNRAS, 499, 1037
Rojas-Arriagada, A., Zoccali, M., Schultheis, M., et al. 2019, A&A, 626, A16
Romano, D., Bellazzini, M., Starkenburg, E., & Leaman, R. 2015, MNRAS, 446, 4220
Romano, D., Karakas, A. I., Tosi, M., & Matteucci, F. 2010, A&A, 522, A32
Romano, D., Matteucci, F., Tosi, M., et al. 2007, MNRAS, 376, 405
Romano, D., Matteucci, F., Zhang, Z.-Y., Ivison, R. J., & Ventura, P. 2019, MNRAS, 490, 2838
Romano, D., Matteucci, F., Zhang, Z. Y., Papadopoulos, P. P., & Ivison, R. J. 2017, MNRAS, 470, 401
Romano, D., & Starkenburg, E. 2013, MNRAS, 434, 471
Saha, A., Vivas, A. K., Olszewski, E. W., et al. 2019, ApJ, 874, 30
Sánchez Almeida, J., Elmegreen, B. G., Muñoz-Tuñón, C., & Elmegreen, D. M. 2014, A&ARv, 22, 71
Saracino, S., Dalessandro, E., Ferraro, F. R., et al. 2019, ApJ, 874, 86
Schmidt, M. 1959, ApJ, 129, 243
Schultheis, M., Rojas-Arriagada, A., García Pérez, A. E., et al. 2017, A&A, 600, A14
Shara, M. M., & Hurley, J. R. 2002, ApJ, 571, 830
Shara, M. M., & Hurley, J. R. 2006, ApJ, 646, 464
Shingles, L. J., Doherty, C. L., Karakas, A. I., et al. 2015, MNRAS, 452, 2804
Springel, V., & Hernquist, L. 2005, ApJL, 622, L9
Surot, F., Valenti, E., Hidalgo, S. L., et al. 2019, A&A, 623, A168
Tinsley, B. M. 1980, Fund. Cosmic Phys., 5, 287
Valenti, E., Zoccali, M., Renzini, A., et al. 2013, A&A, 559, A98
van den Bergh, S. 1962, AJ, 67, 486
Vesperini, E., & Heggie, D. C. 1997, MNRAS, 289, 898
Zoccali, M., Renzini, A., Ortolani, S., et al. 2003, A&A, 399, 931
Zoccali, M., Vasquez, S., Gonzalez, O. A., et al. 2017, A&A, 599, A12